A direct D-bar reconstruction algorithm for recovering a complex conductivity in 2-D

S. J. Hamilton[*], **C. N. L. Herrera**[†], **J. L. Mueller**[‡], and **A. Von Herrmann**[§]

[*]Department of Mathematics, Colorado State University, USA

[†]Department of Mechanical Engineering, University of São Paulo, Brazil

[‡]Department of Mathematics and School of Biomedical Engineering, Colorado State University, USA

[§]Department of Mathematics and Statistics, Colby College, USA

Abstract

A direct reconstruction algorithm for complex conductivities in $W^{2,\infty}(\Omega)$, where Ω is a bounded, simply connected Lipschitz domain in $\mathbb{R}^2$, is presented. The framework is based on the uniqueness proof by Francini [Inverse Problems **20** 2000], but equations relating the Dirichlet-to-Neumann to the scattering transform and the exponentially growing solutions are not present in that work, and are derived here. The algorithm constitutes the first D-bar method for the reconstruction of conductivities and permittivities in two dimensions. Reconstructions of numerically simulated chest phantoms with discontinuities at the organ boundaries are included.

1 Introduction

The reconstruction of admittivies γ from electrical boundary measurements is known as the *inverse admittivity problem*. The unknown admittivity appears as a complex coefficient $\gamma(z) = \sigma(z) + i\omega\varepsilon(z)$ in the generalized Laplace equation

$$\nabla \cdot (\gamma(z)\nabla u(z))=0, \quad z \in \Omega, \quad u|_{\partial\Omega}=f, \quad (1)$$

where u is the electric potential, σ is the conductivity of the medium, ε is the permittivity, and ω is the temporal angular frequency of the applied electromagnetic wave. The data is the Dirichlet-to-Neumann, or voltage-to-current density map defined by

$$\Lambda_\gamma u = \gamma \frac{\partial u}{\partial \nu}\Big|_{\partial\Omega}, \quad (2)$$

where $u \in H^1(\Omega)$ is the solution to (1). By the trace theorem $\Lambda_\gamma: H^{1/2}(\Omega) \to H^{-1/2}(\Omega)$.

In this work we present a direct reconstruction algorithm for the admittivity γ. The majority of the theory is based on the 2000 paper by Francini [21] in which it is established that if σ, $\varepsilon \in W^{2,\infty}(\Omega)$, where Ω is a bounded domain in $\mathbb{R}^2$ with Lipschitz boundary, then the real-valued functions σ and ε are uniquely determined by the Dirichlet-to-Neumann map, provided that the imaginary part of the admittivity is sufficiently small. The proof in [21] is based on the D-bar method and is nearly constructive, but equations linking the scattering transform and the exponentially growing solutions to the Dirichlet-to-Neumann data are not used in the proof, and so it does not contain a complete set of equations for reconstructing the admittivity. In this work, we derive the necessary equations for a direct, nonlinear

reconstruction algorithm for the admittivity γ. Furthermore, we establish the existence of exponentially growing solutions to (1), which prove to be useful in relating the Dirichlet-to-Neumann data to the scattering transform. The reconstruction formula in [21] is for the potential Q_γ, whose relationship to γ is described below. We provide a direct formula for γ from the D-bar equations in [21], which is computationally advantageous as well.

The inverse admittivity problem has an important application known as electrical impedance tomography (EIT). The fact that the electrical conductivity and permittivity vary in the different tissues and organs in the body allows one to form an image from the reconstructed admittivity distribution. In the 2-D geometry, EIT is clinically useful for chest imaging. Conductivity images have been used for monitoring pulmonary perfusion [9, 23, 48], determining regional ventilation in the lungs [24, 22, 52], and the detection of pneumothorax [16], for example. In three dimensions, conductivity images have been used, for instance, in head imaging [51, 50] and knowledge of the admittivity has been applied to breast cancer detection [8, 31, 32].

Reconstruction algorithms based on a least-squares approach that reconstruct permittivity include [19, 8, 30]. The aforementioned algorithms are iterative, whereas the work presented here is a direct method that makes use of exponentially growing solutions, or complex geometrical optics (CGO) solutions, to the admittivity equation. The steps of the algorithm are to compute these CGO solutions from knowledge of the Dirichlet-to-Neumann map, to compute a scattering transform matrix, to solve two systems of $\bar{\partial}$ (D-bar) equations in the complex frequency variable k for the CGO solutions to a related elliptic system, and finally to reconstruct the admittivity from the values of these solutions at $k = 0$. In this work, we provide a complete implementation of this algorithm and present reconstructions of several numerical phantoms relevant to medical EIT imaging. The phantoms we consider here are discontinuous at the organ boundaries, which is actually outside the theory of the algorithm. The work [26] contains computations of smooth admittivities and validates our formulas and computations by comparing the results of the intermediate functions (CGO solutions and scattering transforms) with those computed from knowledge of the admittivity.

We briefly review the history of results using CGO solutions on the inverse conductivity problem in dimension 2. The inverse conductivity problem was first introduced by A.P. Calderón [12] in 1980, where he proved that, in a linearized version of the problem, the Dirichlet-to-Neumann map uniquely determines the conductivity, and he proposed a direct reconstruction method for this case. An implementation in dimension two for experimental data is found in [6]. In 1996, Nachman [44] presented a constructive proof of global uniqueness for twice differentiable conductivities using D-bar methods. The D-bar algorithm following from [44, 46] has been applied to simulated data in [39, 41, 27, 38] and to experimental data on tanks and *in vivo* human data in [28, 29, 42, 18]. While the initial scattering transform was regularized using a Born approximation, a more recent paper [40] contains a full nonlinear regularization analysis, including estimates on speed of convergence in Banach spaces, for twice differentiable conductivities. The regularity conditions on the conductivity were relaxed to once-differentiable in [10]. The proof uses D-bar techniques and formulates the problem as a first-order elliptic system. A reconstruction method based on [10] can be found in [33, 34, 35]. Francini [21] provided a proof of unique identifiability for the inverse admittivity problem for $\sigma, \varepsilon \in W^{2,\infty}(\Omega)$, with ω small. Her work provides a nearly constructive proof based on D-bar methods on a first-order elliptic system similar to that in [10]. A non-constructive proof that applies to complex admittivities with no smallness assumption is found in [11]. Astala and Päivärinta provide a CGO-based constructive proof for real conductivities $\sigma \in L^\infty(\Omega)$, and numerical results related to this work can be found in [3, 4].

The paper is organized as follows. In Section 2 we describe the direct reconstruction algorithm, which is comprised of boundary integral equations for the exponentially growing solutions to (1) involving the Dirichlet-to-Neumann data, boundary integral equations relating those CGO solutions and the CGO solutions Ψ of the first order system, equations for the scattering transform involving only the traces of Ψ, the $\bar{\partial}_k$ equations established in [21], and the direct reconstruction formula for Q_γ and thus γ. Derivations of the novel equations are found in this section. Section 3 describes the numerical implementation of the algorithm. Results on noisy and non-noisy simulated data of a cross-sectional chest with discontinuous organ boundaries are found in Section 4.

2 The Direct Reconstruction Algorithm

In this section we will provide the equations for the direct reconstruction algorithm, completing the steps for the proof in [21] to be completely constructive. In particular, boundary integral equations relating the CGO solutions to the Dirichlet-to-Neumann (DN) map are derived.

Let $\Omega \subset \mathbb{R}^2$ be a bounded open domain with a Lipschitz boundary. Throughout we assume that there exist positive constants σ_0 and β such that

$$\sigma(z) > \sigma_0, \quad z \in \Omega \subset \mathbb{R}^2 \quad (3)$$

and

$$\left\| \sigma \right\|_{W^{1,\infty}(\Omega)}, \left\| \varepsilon \right\|_{W^{1,\infty}(\Omega)} \leq \beta. \quad (4)$$

We extend σ and ε from Ω to all of $\mathbb{R}^2$ such that $\sigma \equiv 1$ and $\varepsilon \equiv 0$ outside a ball with fixed radius that contains Ω, and (3) and (4) hold for all of $\mathbb{R}^2$. In fact, all that is required is that γ is constant outside that ball of fixed radius; for convenience we look at the case where $\gamma \equiv 1$.

The proof in [21] closely follows that of [10] for conductivities $\sigma \in W^{1,p}(\Omega)$, $p > 2$. The matrix potential Q_γ is, however, defined slightly differently, and since the potential in [21] is not Hermitian, the approach in [21] is to consider the complex case as a perturbation from the real case provided the imaginary part of γ is small. Define $Q_\gamma(z)$ and a matrix operator D by

$$Q_\gamma(z) = \begin{pmatrix} 0 & -\frac{1}{2}\partial_z \log\gamma(z) \\ -\frac{1}{2}\bar{\partial}_z \log\gamma(z) & 0 \end{pmatrix}, \quad D = \begin{pmatrix} \bar{\partial}_z & 0 \\ 0 & \partial_z \end{pmatrix}. \quad (5)$$

Thus we define

$$Q_{12}(z) = -\frac{1}{2}\partial_z \log\gamma(z) \quad \text{and} \quad Q_{21}(z) = -\frac{1}{2}\bar{\partial}_z \log\gamma(z), \quad (6)$$

and equivalently we can write

$$Q_{12}(z) = -\frac{\partial_z \gamma^{1/2}(z)}{\gamma^{1/2}(z)} \quad \text{and} \quad Q_{21}(z) = -\frac{\overline{\partial}_z \gamma^{1/2}(z)}{\gamma^{1/2}(z)}, \quad (7)$$

or

$$Q_{12}(z) = -\frac{1}{2}\gamma^{-1}(z)\partial\gamma(z) \quad \text{and} \quad Q_{21}(z) = -\frac{1}{2}\gamma^{-1}(z)\overline{\partial}\gamma(z). \quad (8)$$

Defining a vector

$$\begin{pmatrix} v \\ w \end{pmatrix} = \gamma^{1/2} \begin{pmatrix} \partial u \\ \overline{\partial} u \end{pmatrix}, \quad (9)$$

in terms of the solution u to (1), one sees that

$$D \begin{pmatrix} v \\ w \end{pmatrix} - Q_\gamma \begin{pmatrix} v \\ w \end{pmatrix} = 0.$$

The uniqueness result in [21] is

Theorem 2.1. (Theorem 1.1 [21])—Let Ω be an open bounded domain in $\mathbb{R}^2$ with Lipschitz boundary. Let σ_j and ε_j, for $j = 1, 2$ satisfy assumptions (3) and $\|\sigma\|_{W^{2,\infty}(\Omega)}$, $\|\varepsilon\|_{W^{2,\infty}(\Omega)} \quad \beta$. There exists a constant $\omega_0 = \omega_0(\beta, \sigma_0, \Omega)$ such that if $\gamma_j = \sigma_j + i\omega\varepsilon_j$ for $j = 1, 2$ and $\omega < \omega_0$ and if

$$\Lambda_{\gamma_1} = \Lambda_{\gamma_2},$$

then

$$\sigma_1 = \sigma_2 \quad \text{and} \quad \varepsilon_1 = \varepsilon_2.$$

2.1 CGO solutions

Francini shows in [21] that for ω sufficiently small and γ satisfying (3) and (4) there exists a unique 2×2 matrix $M(z, k)$ for $k \in \mathbb{C}$ satisfying

$$M(\cdot, k) - I \in L^p(\mathbb{R}^2), \quad \text{for some} \quad p > 2, \quad (10)$$

that is a solution to

$$(D_k - Q_\gamma(z))M(z, k) = 0, \quad (11)$$

where D_k is the matrix operator defined by

$$D_k M = DM - ik \begin{pmatrix} 1 & 0 \\ 0 & -1 \end{pmatrix} M^{\text{off}},$$

and "off" denotes the matrix consisting of only the off-diagonal entries of M. The system (11) is equivalent to the following set of equations, included for the reader's convenience

$$\begin{array}{ll} \bar{\partial}_z M_{11} - Q_{12} M_{21} = 0 & (\bar{\partial}_z - ik) M_{12} - Q_{12} M_{22} = 0 \\ (\partial_z + ik) M_{21} - Q_{21} M_{11} = 0 & \partial_z M_{22} - Q_{21} M_{12} = 0. \end{array} \quad (12)$$

Thus, there exists a unique matrix $\Psi(z, k)$ defined by

$$\Psi(z, k) = M(z, k) \begin{pmatrix} e^{izk} & 0 \\ 0 & e^{-i\bar{z}k} \end{pmatrix} = \begin{pmatrix} e^{izk} M_{11}(z, k) & e^{-i\bar{z}k} M_{12}(z, k) \\ e^{izk} M_{21}(z, k) & e^{-i\bar{z}k} M_{22}(z, k) \end{pmatrix}, \quad (13)$$

that is a solution to

$$(D - Q_\gamma) \Psi = 0, \quad (14)$$

or equivalently

$$\begin{array}{ll} \bar{\partial}_z \Psi_{11} - Q_{12} \Psi_{21} = 0 & \partial_z \Psi_{21} - Q_{21} \Psi_{11} = 0 \\ \bar{\partial}_z \Psi_{12} - Q_{12} \Psi_{22} = 0 & \partial_z \Psi_{22} - Q_{21} \Psi_{12} = 0. \end{array} \quad (15)$$

These CGO solutions $\Psi(z, k)$ are key functions in the reconstructions, but the proof in [21] does not provide a link from these functions to the DN data. A useful link can be established through exponentially growing solutions to the admittivity equation (1). For $\gamma - 1$ with compact support, equation (1) can be studied on all of $\mathbb{R}^2$, and introducing the complex parameter k, two distinct exponentially growing solutions, which differ in their asymptotics, exist. We will denote these solutions by u_1 and u_2 where $u_1 \sim \frac{e^{ikz}}{ik}$ and $u_2 \sim \frac{e^{-ik\bar{z}}}{-ik}$ in a sense that is made precise in Theorems 2.2 and 2.3, where the existence of such solutions is established. The proof will make use of the following lemma proved in the real case by Nachman [44]; the complex version shown here also holds and was used in [21]. The lemma is also true if $\bar{}_z$ is interchanged with $_z$.

Lemma 2.1—Let $1 < s < 2$ and $\frac{1}{r} = \frac{1}{s} - \frac{1}{2}$.

1. If the complex function $v \in L^s(\mathbb{R}^2)$, then there exists a unique complex function $u \in L^r(\mathbb{R}^2)$ such that $(_z + ik)u = v$.

2. If the complex function $v \in L^r(\mathbb{R}^2)$ and $\bar{}_z v \in L^s(\mathbb{R}^2)$, $k \in \mathbb{C} \setminus \{0\}$, then there exists a unique complex function $u \in W^{1,r}(\mathbb{R}^2)$ such that $(_z + ik)u = v$.

3. If the complex function $v \in L^r(\mathbb{R}^2)$ and $\bar{}_z v \in L^s(\mathbb{R}^2)$, $k \in \mathbb{C} \setminus \{0\}$, then there exists a unique complex function $u \in W^{1,r}(\mathbb{R}^2)$ such that $(\bar{}_z - ik)u = v$.

The following lemma will also be used in the proofs of Theorems 2.2 and 2.3.

Lemma 2.2—For ω sufficiently small and γ satisfying (3) and (4), the following identities hold:

$$\overline{\partial}_z(\gamma(z)^{-1/2}M_{11}(z,k)-1)=(\partial_z+ik)(\gamma(z)^{-1/2}M_{21}(z,k)) \quad (16)$$

$$\partial_z(\gamma(z)^{-1/2}M_{22}(z,k)-1)=(\overline{\partial}_z-ik)(\gamma(z)^{-1/2}M_{12}(z,k)). \quad (17)$$

Proof: By the product rule,

$$\begin{aligned}
\overline{\partial}_z\left(\gamma(z)^{-1/2}M_{11}(z,k)-1\right) &= \overline{\partial}_z\left(\gamma(z)^{-1/2}\right)M_{11}(z,k)+\gamma(z)^{-1/2}\overline{\partial}_z(M_{11}(z,k)) \\
&= \gamma(z)^{-1/2}Q_{21}(z)M_{11}(z,k)+\gamma(z)^{-1/2}Q_{12}(z)M_{21}(z,k) \\
&= \gamma(z)^{-1/2}(\partial_z+ik)M_{21}(z,k)+\gamma(z)^{-1/2}Q_{12}(z)M_{21}(z,k).
\end{aligned}$$

The second and third equalities utilized (6) and (12), respectively.

We also have

$$\begin{aligned}
(\partial_z+ik)\left(\gamma(z)^{-1/2}M_{21}(z,k)\right) &= \partial_z\left(\gamma(z)^{-1/2}M_{21}(z,k)\right)+ik\gamma(z)^{-1/2}M_{21}(z,k) \\
&= \partial_z\left(\gamma(z)^{-1/2}\right)M_{21}(z,k)+\gamma(z)^{-1/2}\partial_z(M_{21}(z,k))+ik\gamma(z)^{-1/2}M_{21}(z,k) \\
&= \gamma(z)^{-1/2}Q_{12}(z)M_{21}(z,k)+\gamma(z)^{-1/2}(\partial_z+ik)M_{21}(z,k).
\end{aligned}$$

This establishes (16).

Similarly, using (6) and (12),

$$\begin{aligned}
\partial_z\left(\gamma(z)^{-1/2}M_{22}(z,k)-1\right) &= \partial_z\left(\gamma(z)^{-1/2}\right)M_{22}(z,k)+\gamma(z)^{-1/2}\partial_z(M_{22}(z,k)) \\
&= \gamma(z)^{-1/2}Q_{12}(z)M_{22}(z,k)+\gamma(z)^{-1/2}Q_{21}(z)M_{12}(z,k) \\
&= \gamma(z)^{-1/2}(\overline{\partial}_z-ik)M_{12}(z,k)+\gamma(z)^{-1/2}Q_{21}(z)M_{12}(z,k).
\end{aligned}$$

We also have

$$\begin{aligned}
(\overline{\partial}_z-ik)\left(\gamma(z)^{-1/2}M_{12}(z,k)\right) &= \overline{\partial}_z\left(\gamma(z)^{-1/2}M_{12}(z,k)\right)-ik\gamma(z)^{-1/2}M_{12}(z,k) \\
&= \overline{\partial}_z\left(\gamma(z)^{-1/2}\right)M_{12}(z,k)+\gamma(z)^{-1/2}\overline{\partial}_z(M_{12}(z,k))-ik\gamma(z)^{-1/2}M_{12}(z,k) \\
&= \gamma(z)^{-1/2}Q_{21}(z)M_{12}(z,k)+\gamma(z)^{-1/2}(\overline{\partial}_z-ik)M_{12}(z,k).
\end{aligned}$$

This establishes (17).

Knudsen establishes the existence of exponentially growing solutions to the conductivity equation in the context of the inverse conductivity problem in [33]. The proofs of their existence for the admittivity equation and the associated boundary integral equations are in the same spirit as [33].

Theorem 2.2—Let $\gamma(z) \in W^{1,p}(\Omega)$, with $p > 2$ such that σ and ε satisfy (3) and (4), and let $\gamma(z) - 1$ have compact support in $W^{1,p}(\Omega)$. Then for all $k \in \mathbb{C}\backslash\{0\}$ there exists a unique solution

$$u_1(z,k)=e^{ikz}\left[\frac{1}{ik}+w_1(z,k)\right], \quad (18)$$

to the admittivity equation in $\mathbb{R}^2$ such that $w_1(\cdot,k)\in W^{1,r}(\mathbb{R}^2)$, $2<r<\infty$. Moreover, the following equalities hold:

$$(\partial_z+ik)\left[e^{-ikz}u_1(z,k)-\frac{1}{ik}\right]=\gamma^{-1/2}(z)M_{11}(z,k)-1 \quad (19)$$

$$\overline{\partial}_z\left[e^{-ikz}u_1(x,k)-\frac{1}{ik}\right]=\gamma^{-1/2}(z)M_{21}(z,k), \quad (20)$$

and

$$\left\|e^{-ikz}u_1(x,k)-\frac{1}{ik}\right\|_{W^{1,r}(\mathbb{R}^2)}\le C\left(1+\frac{1}{|k|}\right), \quad (21)$$

for some constant C.

Theorem 2.3—Let $\gamma(z)$ satisfy the hypotheses of Theorem 2.2. Then for all $k\in\mathbb{C}\setminus\{0\}$ there exists a unique solution

$$u_2(z,k)=e^{-ik\overline{z}}\left[\frac{1}{-ik}+w_2(z,k)\right], \quad (22)$$

to the admittivity equation in $\mathbb{R}^2$ with $w_2(\cdot,k)\in W^{1,r}(\mathbb{R}^2)$, $2<r<\infty$. Moreover, the following equalities hold:

$$(\overline{\partial}_z-ik)\left[e^{ik\overline{z}}u_2(z,k)+\frac{1}{ik}\right]=\gamma^{-1/2}(z)M_{22}(z,k)-1 \quad (23)$$

$$\partial_z\left[e^{ik\overline{z}}u_2(z,k)+\frac{1}{ik}\right]=\gamma^{-1/2}(z)M_{12}(z,k), \quad (24)$$

and

$$\left\|e^{ik\overline{z}}u_2(z,k)+\frac{1}{ik}\right\|_{W^{1,r}(\mathbb{R}^2)}\le C\left(1+\frac{1}{|k|}\right), \quad (25)$$

for some constant C.

We will prove Theorem 2.2; the proof of Theorem 2.3 is analogous.

Proof: Assume u is a solution of the admittivity equation of the form (18), and let $(v,w)^T=\gamma^{1/2}(\partial_z u,\overline{\partial}_z u)^T$ be the corresponding solution to $(D-Q_\gamma)\Psi=0$. Define the complex function v via $v(z,k)=\gamma(z)^{-1/2}M_{11}(z,k)-1$. We will first show there exists a unique

complex function $w_1 \in W^{1,r}(\mathbb{R}^2)$, where $r > 2$ such that $(\bar{\partial}_z + ik)w = v$, for $k \in \mathbb{C}\setminus\{0\}$. Let us rewrite v as follows:

$$v(z,k) = \gamma(z)^{-1/2}\,[M_{11}(z,k)-1] + \left[\gamma(z)^{-1/2}-1\right].$$

Let $r > 2$ and $1 < s < 2$ with $\frac{1}{r} = \frac{1}{s} - \frac{1}{2}$. We know by Theorem 4.1 of [21] that there exists a constant $C > 0$ depending on β, σ_0 and p such that $\sup \|M_{11}(z,k)-1\|_{L^r(\mathbb{R}^2)} \leq C$ for every $r > 2$, and that $\gamma(z)^{-1/2}-1$ has compact support in $W^{1,r}(\mathbb{R}^2)$. It follows that $v \in L^r(\mathbb{R}^2)$, and by Minkowski's Inequality

$$\left\|v(z,k)\right\|_{L^r} = \left\|\gamma(z)^{-1/2}\,[M_{11}(z,k)-1] + \left[\gamma(z)^{-1/2}-1\right]\right\|_{L^r} \leq C_{r,\gamma},$$

where $C_{r,\gamma}$ depends on r and the bounds on σ and ε.

From (8),

$$\begin{aligned}
\bar{\partial}_z v(z,k) &= \bar{\partial}_z(\gamma(z)^{-1/2}M_{11}(z,k)-1) \\
&= (\bar{\partial}_z\gamma(z)^{-1/2})M_{11}(z,k) + \gamma(z)^{-1/2}(\bar{\partial}_z M_{11}(z,k)) \\
&= \gamma(z)^{-1/2}Q_{21}(z)M_{11}(z,k) + \gamma(z)^{-1/2}Q_{12}(z)M_{21}(z,k) \\
&= \gamma(z)^{-1/2}Q_{21}(z)[M_{11}(z,k)-1] + \gamma(z)^{-1/2}Q_{21}(z) + \gamma(z)^{-1/2}Q_{12}(z)M_{21}(z,k)
\end{aligned}$$

We know that $\gamma(z)^{-1/2}Q_{21}(z) \in L^a(\mathbb{R}^2)$ with $1 \leq a \leq p$ since $Q_{12}(z)$ has compact support. It follows that $\gamma(z)^{-1/2}Q_{21}(z) \in L^s(\mathbb{R}^2) \cap L^2(\mathbb{R}^2)$. By the generalized Hölder's inequality and the fact that $\|M_{11}(z,k)-1\|_{L^s}$ is bounded with $\frac{1}{s} = \frac{1}{r} + \frac{1}{2}$, we have $\bar{\partial}_z v \in L^s(\mathbb{R}^2)$ and $\|\bar{\partial}_z v\|_{L^s(\mathbb{R}^2)} \leq K_{r,\gamma}$, where $K_{r,\gamma}$ depends only on r and the bounds on σ and ε. Thus, by Lemma 2.1 (2), there exists a unique solution $w_1(z,k) \in W^{1,r}(\mathbb{R}^2)$ such that

$$(\partial_z + ik)w_1(z,k) = \gamma(z)^{-1/2}M_{11}(z,k)-1. \quad (26)$$

We have by (16),

$$\bar{\partial}(\gamma(z)^{-1/2}M_{11}(z,k)-1) = (\partial_z + ik)\left(\gamma(z)^{-1/2}M_{21}(z,k)\right). \quad (27)$$

Taking $\bar{\partial}_z$ of both sides of (26) and using (27),

$$\begin{aligned}
\bar{\partial}_z(\partial_z + ik)w_1(z,k) &= \bar{\partial}_z\left(\gamma(z)^{-1/2}M_{11}(z,k)-1\right) \\
&= (\partial_z + ik)\left(\gamma(z)^{-1/2}M_{21}(z,k)\right).
\end{aligned} \quad (28)$$

Using the fact $\bar{\partial}(\cdot + ik) = (\cdot + ik)\bar{\partial}$, it follows that

$$(\partial_z + ik)\left(\bar{\partial}_z w_1(z,k) - \gamma(z)^{-1/2}M_{21}(z,k)\right) = 0. \quad (29)$$

Since $\bar{\partial}_z w_1(z,k) - \gamma(z)^{-1/2}M_{21}(z,k) \in L^r(\mathbb{R}^2)$, by Lemma 2.1 (1), we must have

$$\overline{\partial}_z w_1(z,k) = \gamma(z)^{-1/2} M_{21}(z,k). \quad (30)$$

We now define

$$u_1(z,k) = e^{ikz} \left[w_1(z,k) + \frac{1}{ik} \right], \quad (31)$$

then by (26)

$$(\partial_z + ik) \left(e^{-ikz} u_1(z,k) - \frac{1}{ik} \right) = (\partial_z + ik) \, w_1(z,k) = \gamma^{-1/2}(z) M_{11}(z,k) - 1,$$

which proves (19), and by (30)

$$\overline{\partial}_z \left(e^{-ikz} u_1(z,k) - \frac{1}{ik} \right) = \overline{\partial}_z w_1(z,k) = \gamma^{-1/2}(z) M_{21}(z,k),$$

which proves (20).

The norm estimate given by (21) follows by Minkowski's Inequality, the constant C depends on r, the bound on $\gamma - 1$, and the bounds on σ and ε.

Remark

Note that from (19)

$$\begin{aligned}
\gamma^{-1/2} M_{11}(z,k) - 1 &= (\partial_z + ik) \left(e^{-ikz} u_1(z,k) - \frac{1}{ik} \right) \\
&= \partial_z (e^{-ikz} u_1) + ik e^{-ikz} u_1(z,k) - 1 \qquad (32) \\
&= e^{-ikz} \partial_z u_1(z,k) - 1,
\end{aligned}$$

and from (20)

$$\begin{aligned}
\gamma^{-1/2} M_{21}(z,k) &= \overline{\partial}_z \left(e^{-ikz} u_1(z,k) - \frac{1}{ik} \right) \\
&= u_1(z,k) \overline{\partial}_z (e^{-ikz}) + e^{-ikz} \overline{\partial}_z u_1(z,k) \qquad (33) \\
&= e^{-ikz} \overline{\partial}_z u_1(z,k).
\end{aligned}$$

Thus, we can equivalently rewrite (19) and (20), respectively, as

$$\gamma^{1/2}(z) \, \partial_z u_1(z,k) = e^{ikz} M_{11}(z,k) = \Psi_{11}(z,k) \quad (34)$$

$$\gamma^{1/2}(z) \overline{\partial}_z u_1(z,k) = e^{ikz} M_{21}(z,k) = \Psi_{21}(z,k). \quad (35)$$

In a similar manner, we can rewrite (23) and (24), respectively, as

$$\gamma^{1/2}(z)\overline{\partial}_z\, u_2(z,k)=e^{-ik\overline{z}}M_{22}(z,k)=\Psi_{22}(z,k) \quad (36)$$

$$\gamma^{1/2}(z)\, \partial_z\, u_2(z,k)=e^{-ik\overline{z}}M_{12}(z,k)=\Psi_{12}(z,k). \quad (37)$$

Useful boundary integral equations for the traces of u_1 and u_2 can be derived under the additional assumption that $\gamma \in W^{2,p}$ and $u_1,\, u_2 \in W^{2,p},\, p>1$. The following proposition shows a relationship between the exponentially growing solutions $\psi_S(z,k)$ (when they exist) to the Schrödinger equation

$$(-\Delta+q_S(z))\psi_S(z,k)=0, \quad (38)$$

and the CGO solutions u_1 and u_2 to (1). The solution ψ_S to (38), where q_S is complex, is asymptotic to e^{ikz} in the sense that

$$w_S \equiv e^{-ikz}\psi_S(\cdot,k)-1 \in L^{\overline{p}} \cap L^{\infty},$$

where $\frac{1}{\overline{p}}=\frac{1}{p}-\frac{1}{2}$ and $1<p<2$. The question of the existence of a unique solution to (38) is addressed for real γ in [44], where it is shown to exist if and (roughly) only if $q_s=\frac{\Delta\gamma^{1/2}}{\gamma^{1/2}}$. The solutions ψ_S will be used to derive the boundary integral equations for u_1 and u_2, but not in the direct reconstruction algorithm.

Lemma 2.3—Let $\gamma(z) = \sigma(z) + i\omega\varepsilon(z) \in W^{2,p}(\Omega)$, with $p>2$ such that σ and ε satisfy (3) and (4), and let $\gamma(z) - 1$ have compact support in $W^{1,p}(\Omega)$. Let u_1 be the exponentially growing solution to the admittivity equation as given in Theorem 2.2, and let ψ_S be the exponentially growing solution to the Schrödinger equation (38), when it exists. Then

$$iku_1(z,k)=\gamma^{-1/2}(z)\psi_S(z,k). \quad (39)$$

Proof: From (18),

$$\begin{aligned}
iku_1(z,k)&=e^{ikz}(1+ikw_1(z,k))\\
&=e^{ikz}\gamma^{-1/2}(z)\left[\gamma^{1/2}(z)+\gamma^{1/2}(z)ikw_1(z,k)\right]\\
&=e^{ikz}\gamma^{-1/2}(z)\left(1+\left[\gamma^{1/2}(z)-1\right]+\gamma^{1/2}(z)ikw_1(z,k)\right)
\end{aligned}$$

satisfies the admittivity equation with $[\gamma^{1/2}(z)-1]+\gamma^{1/2}(z)ikw_1(z,k) \in W^{1,r}(\Omega)$ for $r>2$. We also know that when it exists,

$$\gamma^{-1/2}(z)\psi_S(z,k)=e^{ikz}\gamma^{-1/2}(z)(1+w_S(z,k)) \quad (40)$$

is also a solution to the admittivity equation with $w_S(z,k) \in W^{1,\overline{p}}(\mathbb{R}^2)$. Hence, these exponentially growing solutions must be equal.

Lemma 2.4—Let $\gamma(z) = \sigma(z) + i\omega\varepsilon(z) \in W^{2,p}(\Omega)$, with $p > 2$ such that σ and ε satisfy (3) and (4), and let $\gamma(z) - 1$ have compact support in $W^{1,p}(\Omega)$. Let u_2 be the exponentially growing solution to the admittivity equation as given in Theorem 2.3, and let ψ_S be the exponentially growing solution to the Schrödinger equation (38), when it exists. Then

$$-iku_2(z, k) = \gamma^{-1/2}(-\bar{z})\psi_S(-\bar{z}, k). \quad (41)$$

Proof: From (22),

$$-iku_2(z, k) = e^{-ik\bar{z}}(1 - ikw_2(z, k))$$
$$= e^{-ik\bar{z}}\gamma^{-1/2}(-\bar{z})\left(1 + \left[\gamma^{1/2}(-\bar{z}) - 1\right] - \gamma^{1/2}(-\bar{z})ikw_2(z, k)\right)$$

satisfies the admittivity equation with $[\gamma^{1/2}(-\bar{z}) - 1] - \gamma^{1/2}(-\bar{z})ikw_2(z, k) \in W^{1,r}(\Omega)$ for $r > 2$. From (40),

$$\gamma^{1/2}(-\bar{z})\psi_S(-\bar{z}, k) = e^{-ik\bar{z}}\gamma^{1/2}(-\bar{z})(1 + w_S(-\bar{z}, k))$$

satisfies the admittivity equation with $w_S(-\bar{z}, k) \in W^{1,\bar{p}}(\mathbb{R}^2)$. Thus, these exponentially growing solutions must be equal, and so

$$-iku_2(z, k) = \gamma^{-1/2}(-\bar{z})\psi_S(-\bar{z}, k).$$

Let us recall some terminology arising from [44] before establishing boundary integral equations involving the exponentially growing solutions. Let Λ_σ be the Dirichlet-to-Neumann map when Ω contains the conductivity distribution σ, and Λ_1 is the Dirichlet-to-Neumann map for a homogeneous conductivity equal to 1. The Faddeev Green's function $G_k(z)$ is defined by

$$G_k(z) := e^{ik \cdot z} g_k(z), \quad -\Delta G_k = \delta, \quad (42)$$

where

$$g_k(z) := \frac{1}{(2\pi)^2} \int_{\mathbb{R}^2} \frac{e^{iz \cdot \xi}}{\xi(\bar{\xi} + 2k)} d\xi, \quad (-\Delta - 4ik\bar{\partial})g_k = \delta, \quad (43)$$

for $k \in \mathbb{C}\backslash\{0\}$. In the real-valued case $\gamma = \sigma$, the trace of the function $\psi_S(\cdot, k)$ on $\partial\Omega$ satisfies the integral equation [44]

$$\psi_S(z, k) = e^{ikz} - \int_{\partial\Omega} G_k(z - \zeta)(\Lambda_\sigma - \Lambda_1)\psi_S(\zeta, k)dS(\zeta), \quad z \in \partial\Omega, \quad (44)$$

where $k \in \mathbb{C}\backslash\{0\}$. The equation (44) is a Fredholm equation of the second kind and uniquely solvable in $H^{1/2}(\partial\Omega)$ for any $k \in \mathbb{C}\backslash\{0\}$.

The boundary integral equations for u_1 and u_2 are similar to (44).

Theorem 2.4—Let $\gamma \in W^{2,p}(\Omega)$ for $p > 1$ and suppose $\gamma = 1$ in a neighborhood of Ω. Suppose σ and ε satisfy (3) and (4), and let $\gamma(z) - 1$ have compact support in $W^{2,p}(\Omega)$. Then for any nonexceptional $k \in \mathbb{C}\backslash\{0\}$, the trace of the exponentially growing solution $u_1(\cdot, k)$ on Ω is the unique solution to

$$u_1(z,k) = \frac{e^{ikz}}{ik} - \int_{\partial\Omega} G_k(z-\zeta)(\Lambda_\gamma - \Lambda_1)u_1(\zeta,k)dS(\zeta), \quad z \in \partial\Omega. \quad (45)$$

Proof: Let $\frac{1}{p} = \frac{1}{r} - \frac{1}{2}$, where $1 < r < 2$ and $p > 2$. Let $\{\gamma_n\}_{n \in \mathbb{N}} \subset W^{2,r}(\Omega)$ be a sequence converging to $\gamma \in W^{1,p}(\Omega)$. Then by the Sobolev Embedding Theorem, $\{\gamma_n\}_{n \in \mathbb{N}} \subset W^{1,r}(\Omega)$. Let ψ_n be the exponentially growing solutions to the Schrödinger equation with potential $\gamma_n^{-1/2}\Delta\gamma_n^{1/2}$, and u^n be the CGO solutions defined by Theorem 2.2 to the admittivity equation with admittivity γ_n. Then for each $n \in \mathbb{N}$, the complex γ version of (44) holds for nonexceptional $k \in \mathbb{C}\backslash\{0\}$

$$\psi_n(z,k)|_{\partial\Omega} = e^{ikz}|_{\partial\Omega} - \int_{\partial\Omega} G_k(z-\zeta)(\Lambda_{\gamma_n} - \Lambda_1)\psi_n(\zeta,k)dS(\zeta), \quad (46)$$

where $\gamma_n = 1$ in the neighborhood of Ω.

It follows by (39) that for each complex number $k \neq 0$, and for each $n \in \mathbb{N}$

$$\frac{\gamma_n^{-1/2}(z)}{ik}\psi_n(z,k) = u^n(z,k) \to u_1(z,k) \quad \text{in} \quad H^{1/2}(\partial\Omega). \quad (47)$$

We claim that for each n, u^n satisfies (45). To see this, by (39), for $z \in \Omega$,

$$
\begin{aligned}
&\frac{e^{ikz}}{ik} - \int_{\partial\Omega} G_k(z-\zeta)(\Lambda_\gamma - \Lambda_1)u^n(\zeta,k)dS(\zeta) \\
&= \frac{e^{ikz}}{ik} - \int_{\partial\Omega} G_k(z-\zeta)(\Lambda_\gamma - \Lambda_1)\frac{\gamma_n^{-1/2}(\zeta)}{ik}\psi_n(\zeta,k)dS(\zeta) \\
&\qquad\qquad = \frac{\gamma_n^{-1/2}(z)}{ik}\psi_n(z,k) \\
&\qquad\qquad = u^n(z,k),
\end{aligned}
\quad (48)
$$

where we used the fact that $\gamma_n = 1$ in a neighborhood of Ω. Thus, u^n satisfies (45) for each $n \in \mathbb{N}$.

We know by Theorem 3.1 of [21] that $M(z, k)$ depends continuously on γ. From (47), we can conclude that

$$\int_{\partial\Omega} G_k(z-\zeta)(\Lambda_{\gamma_n} - \Lambda_1)u^n(\zeta,k)dS(\zeta) \mapsto \int_{\partial\Omega} G_k(z-\zeta)(\Lambda_\gamma - \Lambda_1)u_1(\zeta,k)dS(\zeta). \quad (49)$$

Thus, by (47), (48), and (49), we have that $u_1(\cdot, k)|_\Omega$ satisfies (45). The uniqueness of $u_1(\cdot, k)|_\Omega$ follows by Theorem 2.2.

An analogous theorem holds for u_2.

Theorem 2.5—Let $\gamma \in W^{2,p}(\Omega)$ for $p > 1$ and suppose $\gamma = 1$ in a neighborhood of $\partial\Omega$. Suppose σ and ε satisfy (3) and (4), and let $\gamma(z) - 1$ have compact support in $W^{2,p}(\Omega)$. Then for any nonexceptional $k \in \mathbb{C}\backslash\{0\}$, the trace of the exponentially growing solution $u_2(\cdot, k)$ on $\partial\Omega$ is the unique solution to

$$u_2(z, k) = \frac{e^{-ik\bar{z}}}{-ik} - \int_{\partial\Omega} G_k(-\bar{z}+\bar{\zeta})(\Lambda_\gamma - \Lambda_1)u_2(\zeta, k)dS(\zeta), \quad z \in \partial\Omega. \quad (50)$$

<u>Proof:</u> Let p, r, $\{\gamma_n\}_{n\in\mathbb{N}} \subset W^{2,r}(\Omega)$, and ψ_n be as in the proof of Theorem 2.4. Let u^n be the CGO solutions defined in Theorem 2.3 to the admittivity equation with admittivity γ_n. Then for each $n \in \mathbb{N}$, for nonexceptional $k \in \mathbb{C}\backslash\{0\}$, evaluating (46) at $-\bar{z}$,

$$\psi_n(-\bar{z}, k)|_{\partial\Omega} = e^{-ik\bar{z}}|_{\partial\Omega} - \int_{\partial\Omega} G_k(-\bar{z}-\zeta)(\Lambda_{\gamma_n} - \Lambda_1)\psi_n(\zeta, k)dS(\zeta), \quad (51)$$

where $\gamma_n = 1$ in a neighborhood of $\partial\Omega$.

It follows by (41) that for each complex number $k \neq 0$, and for each $n \in \mathbb{N}$

$$\frac{\gamma_n^{-1/2}(-\bar{z})}{-ik}\psi_n(-\bar{z}, k) = u^n(z, k) \to u_2(z, k) \quad \text{in} \quad H^{1/2}(\partial\Omega). \quad (52)$$

We claim that for each n, u^n satisfies (50). To see this, by (41), for $z \in \partial\Omega$,

$$\begin{aligned}
&\frac{e^{-ik\bar{z}}}{-ik} - \int_{\partial\Omega} G_k(-\bar{z}+\bar{\zeta})(\Lambda_\gamma - \Lambda_1)u^n(\zeta, k)dS(\zeta) \\
&= \frac{e^{-ik\bar{z}}}{-ik} - \int_{\partial\Omega} G_k(-\bar{z}+\bar{\zeta})(\Lambda_\gamma - \Lambda_1)\frac{\gamma_n^{-1/2}(-\bar{\zeta})}{-ik}\psi_n(-\bar{\zeta}, k)dS(\zeta) \\
&= \frac{e^{-ik\bar{z}}}{-ik} - \int_{\partial\Omega} G_k(-\bar{z}-\bar{\zeta})(\Lambda_\gamma - \Lambda_1)\frac{\gamma_n^{-1/2}(\tilde{\zeta})}{-ik}\psi_n(\tilde{\zeta}, k)dS(\tilde{\zeta}) \\
&= \frac{\gamma_n^{-1/2}(-\bar{z})}{-ik}\psi_n(-\bar{z}, k) \\
&= u^n(z, k),
\end{aligned} \quad (53)$$

using the change of variables $-\bar{\zeta} \mapsto \tilde{\zeta}$ and the fact that $\gamma_n = 1$ in a neighborhood of $\partial\Omega$. Thus, u^n satisfies (50) for each $n \in \mathbb{N}$.

We know by Theorem 3.1 of [21] that $M(z, k)$ depends continuously on γ. From (52), we can conclude that

$$\int_{\partial\Omega} G_k(-\bar{z}+\bar{\zeta})(\Lambda_{\gamma_n} - \Lambda_1)u^n(\zeta, k)dS(\zeta) \mapsto \int_{\partial\Omega} G_k(-\bar{z}+\bar{\zeta})(\Lambda_\gamma - \Lambda_1)u_2(\zeta, k)dS(\zeta). \quad (54)$$

Thus, by (52), (53), and (54), we have that $u_2(\cdot, k)|_{\partial\Omega}$ satisfies (50). The uniqueness of $u_2(\cdot, k)|_{\partial\Omega}$ follows by Theorem 2.3.

2.2 The Scattering Transform Matrix

The scattering transform $S_\gamma(k)$ of the matrix potential Q_γ is defined in [21] by

$$S_\gamma(k) = \frac{i}{\pi}\int_{\mathbb{R}^2} \begin{pmatrix} 0 & Q_{12}(z)e(z, -\bar{k})M_{22}(z, k) \\ -Q_{21}(z)e(z, k)M_{11}(z, k) & 0 \end{pmatrix} d\mu(z), \quad (55)$$

where $e(z, k) = \exp\{i(zk + \bar{z}\bar{k})\}$. Thus we are only concerned with computing the off-diagonal entries of S_γ, which we will denote by $S_{12}(k)$ and $S_{21}(k)$.

Boundary integral formulas for the off-diagonal entries of $S_\gamma(k)$ in (55) can be computed by integration by parts as follows

$$
\begin{aligned}
S_{12}(k) &= \frac{i}{\pi} \int_\Omega Q_{12}(z) e^{-i\bar{k}z} \Psi_{22}(z, k) \, d\mu(z) \\
&= \frac{i}{\pi} \int_\Omega e^{-i\bar{k}z} \overline{\partial}_z \Psi_{12}(z, k) \, d\mu(z) \\
&= \frac{i}{2\pi} \int_{\partial\Omega} e^{-i\bar{k}z} \Psi_{12}(z, k)(\nu_1 + i\nu_2) \, dS(z) - \frac{i}{\pi} \int_\Omega \overline{\partial}_z e^{-i\bar{k}z} \Psi_{12}(z, k) \, d\mu(z) \\
&= \frac{i}{2\pi} \int_{\partial\Omega} e^{i\bar{k}z} \Psi_{12}(z, k)(\nu_1 + i\nu_2) \, dS(z)
\end{aligned}
\tag{56}
$$

and similarly,

$$
S_{21}(k) = -\frac{i}{2\pi} \int_{\partial\Omega} e^{i\overline{kz}} \Psi_{21}(z, k)(\nu_1 - i\nu_1) \, dS(z), \tag{57}
$$

where $\nu = \nu_1 + i\nu_2$ denotes the outward unit normal to the boundary Ω.

Theorem 2.6—The trace of the exponentially growing solutions $\Psi_{12}(z, k)$ and $\Psi_{21}(z, k)$ for $k \in \mathbb{C} \backslash \{0\}$ can be determined by

$$
\Psi_{12}(z, k) = \int_{\partial\Omega} \frac{e^{i\bar{k}(z-\zeta)}}{4\pi(z-\zeta)} [\Lambda_\gamma - \Lambda_1] u_2(\zeta, k) \, dS(\zeta) \tag{58}
$$

$$
\Psi_{21}(z, k) = \int_{\partial\Omega} \overline{\left[\frac{e^{ik(z-\zeta)}}{4\pi(z-\zeta)}\right]} [\Lambda_\gamma - \Lambda_1] u_1(\zeta, k) \, dS(\zeta), \tag{59}
$$

where u_1 and u_2 are calculated via equations (45) and (50) respectively.

Proof: We use the relations in (35) and (37) to obtain boundary integral equations for Ψ_{21} and Ψ_{12} for $z \in \Omega$ from Equations (45) and (50), respectively. Let us begin with Ψ_{12}:

$$
\begin{aligned}
\Psi_{12}(z, k) &= \gamma^{1/2}(z) \, \partial_z u_2(z, k) \\
&= \gamma^{1/2}(z) \, \partial_z \left[\frac{e^{-ikz}}{-ik} - \int_{\partial\Omega} G_k(-\bar{z} + \bar{\zeta}) [\Lambda_\gamma - \Lambda_1] u_2(\zeta, k) \, dS(\zeta) \right] \\
&= -\gamma^{1/2}(z) \int_{\partial\Omega} \partial_z [G_k(-\bar{z} + \bar{\zeta})] [\Lambda_\gamma - \Lambda_1] u_2(\zeta, k) \, dS(\zeta).
\end{aligned}
\tag{60}
$$

Similarly,

$$
\begin{aligned}
\Psi_{21}(z, k) &= \gamma^{1/2}(z) \, \overline{\partial}_z u_1(z, k) \\
&= \gamma^{1/2}(z) \, \overline{\partial}_z \left[\frac{e^{ikz}}{ik} - \int_{\partial\Omega} G_k(z - \zeta) [\Lambda_\gamma - \Lambda_1] u_1(\zeta, k) \, dS(\zeta) \right] \\
&= -\gamma^{1/2}(z) \int_{\partial\Omega} \overline{\partial}_z [G_k(z - \zeta)] [\Lambda_\gamma - \Lambda_1] u_1(\zeta, k) \, dS(\zeta).
\end{aligned}
\tag{61}
$$

A thorough study of the properties of the Faddeev Green's function G_k and its derivatives is given in [47]. The calculations for the specific derivatives needed here are shown below. By the definition of G_k (42)

$$\partial_z\, G_k(-\bar{z}+\bar{\zeta})=\partial_z\left[e^{ik(-\bar{z}+\bar{\zeta})}g_k(-\bar{z}+\bar{\zeta})\right]=e^{ik(-z+\bar{\zeta})}\partial_z\, g_k(-\bar{z}+\bar{\zeta}). \quad (62)$$

Using the definition of g_k (43),

$$\begin{aligned}
\partial_z\, g_k(-\bar{z}+\bar{\zeta}) &=\partial_z \frac{1}{(2\pi)^2}\int_{\mathbb{R}^2}\frac{e^{i(-\bar{z}+\bar{\zeta})\cdot\xi}}{\xi(\bar{\xi}+2k)}d\xi \\
&=\frac{1}{(2\pi)^2}\int_{\mathbb{R}^2}\frac{\partial_z\left[e^{-(i/2)(\bar{z}\xi+z\xi)}\right]e^{i\bar{\xi}\cdot\xi}}{\xi(\bar{\xi}+2k)}d\xi \\
&=\frac{1}{(2\pi)^2}\int_{\mathbb{R}^2}\frac{(i\xi/2)\,e^{i(-\bar{z}+\bar{\zeta})\cdot\xi}}{\xi(\bar{\xi}+2k)}d\xi \\
&=\frac{e^{i(-\bar{z}+\bar{\zeta})\cdot(-2\bar{k})}}{4}\frac{1}{(2\pi)^2}\int_{\mathbb{R}^2}\frac{2e^{i(-\bar{z}+\bar{\zeta})\cdot(\xi+2\bar{k})}}{i\left(\bar{\xi}+2\bar{k}\right)}d\xi \quad (63) \\
&=\frac{e^{i(-\bar{z}+\bar{\zeta})\cdot(-z\bar{k})}}{4\pi\left(-\bar{z}+\bar{\zeta}\right)} \\
&=-\frac{e^{-ik(-\bar{z}+\bar{\zeta})}e^{-i\bar{k}(-z+\zeta)}}{4\pi(z-\zeta)}
\end{aligned}$$

by the definition of the inverse Fourier transform and the well known result

$$\mathscr{F}^{-1}\left\{\frac{2}{i\bar{\xi}}\right\}^{\wedge}(z)-\frac{1}{\pi\bar{z}}.$$

Therefore, by (62) and (63)

$$\partial_z\, G_k(-\bar{z}+\bar{\zeta})=-\frac{e^{i\bar{k}(z-\zeta)}}{4\pi(z-\zeta)}. \quad (64)$$

The $\bar{}_z$ derivative for Ψ_{21} is calculated in a similar manner,

$$\overline{\partial}_z\, G_k(z-\zeta)=-\overline{\left[\frac{e^{ik(z-\zeta)}}{4\pi(z-\zeta)}\right]}. \quad (65)$$

Substituting the representations for $\partial_z\, G_k(-\bar{z}+\bar{\zeta})$ and $\bar{\partial}_z\, G_k(z-\zeta)$, given in (64) and (65), back into the equations for Ψ_{12} and Ψ_{21}, given in (60) and (61) respectively, proves the theorem.

2.3 From *S*(*k*) to *M*

The dependence of M on the complex parameter k is related to the scattering transform through the following $\bar{}_k$ system.

Theorem 2.7 (Theorem 4.1 [21])—Let σ and ε satisfy (3) and (4) and let M be the unique solution to (11) satisfying (10). The map $k \to M(\cdot,\, k)$ is differentiable as a map into $L^r_{-\beta}$, and satisfies the equation

$$\overline{\partial}_k M(z,k)=M(z,\bar{k})\begin{pmatrix} e(z,\bar{k}) & 0 \\ 0 & e(z,-k) \end{pmatrix} S_\gamma(k), \quad (66)$$

where

$$S_\gamma(k) = \frac{i}{\pi} \int_{\mathbb{R}^2} \begin{pmatrix} e(z, -\bar{k}) & 0 \\ 0 & -e(z, k) \end{pmatrix} (Q_\gamma M)^{off}(z, k) \, d\mu(z). \quad (67)$$

Moreover, for every $p > 2$,

$$\sup_k \left\| M(z, \cdot) - I \right\|_{L^p(\mathbb{R}^2)} \leq K_2,$$

where K_2 depends on β, σ_0, Ω, and p.

Notice that Equation (66) can be written as the following two systems of equations:

$$\begin{cases} \bar{\partial}_k M_{11}(z, k) = M_{12}(z, \bar{k}) e(z, -k) S_{21}(k) \\ \bar{\partial}_k M_{12}(z, k) = M_{11}(z, \bar{k}) e(z, \bar{k}) S_{12}(k) \end{cases}, \quad (68)$$

and

$$\begin{cases} \bar{\partial}_k M_{21}(z, k) = M_{22}(z, \bar{k}) e(z, -k) S_{21}(k) \\ \bar{\partial}_k M_{22}(z, k) = M_{21}(z, \bar{k}) e(z, \bar{k}) S_{12}(k) \end{cases}, \quad (69)$$

included for the reader's convenience.

2.4 From *M* to *γ*

Theorem 2.8 (Theorem 6.2 [21])—For any $\rho > 0$,

$$Q_\gamma(z) = \lim_{k_0 \to \infty} \mu(B_\rho(0))^{-1} \int_{\{k : |k - k_0| < \rho\}} D_k M(z, k) d\mu(k). \quad (70)$$

This provides a reconstruction formula for the entries of Q_γ, and one can recover γ from $Q_{12} = -\frac{1}{2}\partial_z \log(\gamma)$ or $Q_{21} = -\frac{1}{2}\bar{\partial}_z \log(\gamma)$. However, this formula is computationally impractical as it requires a large k limit of integrals involving $\bar{\partial}_z$ and ∂_z derivatives of $M(z, k)$.

We have derived computationally advantageous formulas for recovering the entries of Q_γ that only require knowledge of the CGO solutions at $k = 0$. Theorem 2.9 provides this direct relation between the CGO solutions $M(z, 0)$ (from the $\bar{\partial}_k$ equation (66)) and the matrix potential $Q_\gamma(z)$, eliminating the large k limit required in equation (70) above.

Theorem 2.9—The entries of the potential matrix $Q_\gamma(z)$ defined in (5) can be calculated using only knowledge of the CGO solutions $M(z, 0)$ via

$$Q_{12}(z) = \frac{\bar{\partial}_z M_+(Q_\gamma, z, 0)}{M_-(Q_\gamma, z, 0)} \quad (71)$$

$$Q_{21}(z) = \frac{\partial_z M_-(Q_\gamma, z, 0)}{M_+(Q_\gamma, z, 0)}. \quad (72)$$

where,

$$M_+(Q_\gamma, z, k) = M_{11}(Q_\gamma, z, k) + e(z, -k) M_{12}(Q_\gamma, z, k) \quad (73)$$

$$M_-(Q_\gamma, z, k) = M_{22}(Q_\gamma, z, k) + e(z, k) M_{21}(Q_\gamma, z, k). \quad (74)$$

Proof: We follow an idea similar to that in [5] and define

$$M_+(Q_\gamma, z, k) = M_{11}(Q_\gamma, z, k) + e(z, -k) M_{12}(Q_\gamma, z, k) \quad (75)$$

$$M_-(Q_\gamma, z, k) = M_{22}(Q_\gamma, z, k) + e(z, k) M_{21}(Q_\gamma, z, k). \quad (76)$$

Note that M_+ and M_- are only dependent on the Q_γ matrix, not $-Q_\gamma^T$ as is required in [5]. Therefore,

$$\overline{\partial}_z M_+(Q_\gamma, z, k) = Q_{12}(z) e(z, -k) \left[M_-(Q_\gamma, z, k) = +i(k-\overline{k}) M_{12}(Q_\gamma, z, k) \right]$$
$$\partial_z M_-(Q_\gamma, z, k) = Q_{21}(z) e(z, k) M_+(Q_\gamma, z, k),$$

so that

$$\overline{\partial}_z M_+(Q_\gamma, z, 0) = Q_{12}(z) M_-(Q_\gamma, z, 0)$$
$$\partial_z M_-(Q_\gamma, z, 0) = Q_{21}(z) M_+(Q_\gamma, z, 0).$$

One can then reconstruct the log of the admittivity γ from either Q_{12} or Q_{21} by inverting the ∂_z or $\overline{\partial}_z$ operator respectively, and exponentiate to recover explicitly

$$\log(\gamma(z)) = -\frac{2}{\pi} \int_{\mathbb{C}} \frac{Q_{12}(\zeta)}{\overline{z}-\zeta} d\mu(\zeta) = -\frac{2}{\pi} \int_{\mathbb{C}} \frac{Q_{21}(\zeta)}{z-\zeta} d\mu(\zeta). \quad (77)$$

2.5 The steps of the algorithm

We now have all the necessary steps for a direct reconstruction algorithm:

1. Compute the exponentially growing solutions $u_1(z, k)$ and $u_2(z, k)$ to the admittivity equation from the boundary integral formulas (45) and (50)

$$u_1(z, k)|_{\partial\Omega} = \frac{e^{ikz}}{ik}\Big|_{\partial\Omega} - \int_{\partial\Omega} G_k(z-\zeta)(\Lambda_\gamma - \Lambda_1) u_1(\zeta, k) dS(\zeta)$$
$$u_2(z, k)|_{\partial\Omega} = \frac{e^{ik\overline{z}}}{-ik}\Big|_{\partial\Omega} - \int_{\partial\Omega} G_k(-\overline{z}+\overline{\zeta})(\Lambda_\gamma - \Lambda_1) u_2(\zeta, k) dS(\zeta).$$

2. Compute the off diagonal entries of the CGO solution $\Psi(z, k)$ for $z \in \Omega$ from the boundary integral formulas (58) and (59)

$$\Psi_{12}(z,k) = \int_{\partial\Omega} \frac{e^{i\bar{k}(z-\zeta)}}{4\pi(z-\zeta)} [\Lambda_\gamma - \Lambda_1] u_2(\zeta, k) \, dS(\zeta)$$

$$\Psi_{21}(z,k) = \int_{\partial\Omega} \overline{\left[\frac{e^{ik(z-\zeta)}}{4\pi(z-\zeta)} \right]} [\Lambda_\gamma - \Lambda_1] u_1(\zeta, k) \, dS(\zeta).$$

3. Compute the off-diagonal entries of the scattering matrix $S_\gamma(k)$ from (56) and (57)

$$S_{12}(k) = \frac{i}{2\pi} \int_{\partial\Omega} e^{-i\bar{k}z} \Psi_{12}(z,k)(\nu_1 + i\nu_2) dS(z)$$

$$S_{21}(k) = -\frac{i}{2\pi} \int_{\partial\Omega} e^{i\bar{k}z} \Psi_{21}(z,k)(\nu_1 - i\nu_2) dS(z).$$

4. Solve the $\bar{\partial}_k$ equation (66) for the matrix $M(z, k)$

$$\bar{\partial}_k M(z,k) = M(z,\bar{k}) \begin{pmatrix} e(z,\bar{k}) & 0 \\ 0 & e(z,-k) \end{pmatrix} S_\gamma(k).$$

5. Reconstruct Q_γ from Theorem 2.9 and use (77) to compute γ.

3 Numerical Implementation

In this section, we describe the implementation of the algorithm. Greater detail of the numerical methods and validations of the computations for admittivity distributions with twice differentiable real and imaginary parts can be found in [26], where the solution to the forward problem (11) is computed and used to validate formulas (58) an (59), as well as computations of the scattering transform. In this work, we consider examples with discontinuities at the organ boundaries.

3.1 Computation of the DN map

An approximation to the DN map was computed by simulating voltage data by the finite element method (FEM), and then computing a matrix approximation to the map by computing the inner product of the applied currents with the voltages. This approximation to the DN map has been discussed, for example, in [28, 18, 40]. It can be formed analogously in the complex case.

Gaussian white noise was added independently to the real and imaginary parts of the simulated voltages for each current pattern by adding a random vector of amplitude $\eta > 0$ multiplied by the maximum voltage value for that current pattern and real or imaginary component to the computed voltages. We consider noise levels $\eta = 0$ and $\eta = 0.0001$, which corresponds to 0.01% noise, the published level of the ACT 3 system [19], which applies the trigonometric current patterns used in the simulations here.

3.2 Computation of the CGO solutions and $S_\gamma(k)$

The CGO solutions on the boundary of Ω were computed for each k in a grid $[-K, K]^2$ in the complex plane. The choice of K, which serves as a cut-off frequency, was determined by the behavior of the scattering transforms S_{12} and S_{21}. As in [40] for the D-bar algorithm for conductivity reconstructions, the cutoff frequency K has a regularizing effect, and was chosen here empirically to balance smoothing and numerical error. We do not address the selection of K by more sophisticated means in this work.

3.2.1 Computation of u_1 and u_2—A boundary integral equation of the form (45) was solved in [18] and [40]. In this work, as in [18], we employ an approximation to the Faddeev's Green's function G_k that allows for very rapid computation of u_1 and u_2 from (45) and (50) respectively. Namely, G_k is approximated by the fundamental solution for the Laplacian

$$G_0(z) = \frac{1}{2\pi}\log|z|.$$

Denoting the solutions to (45), (50) by u_1^0 and u_2^0, respectively, the convolution integrals

$$u_1^0(z,k)|_{\partial\Omega} = \frac{e^{ikz}}{ik}\Big|_{\partial\Omega} - \int_{\partial\Omega} G_0(z-\zeta)(\Lambda_\gamma - \gamma_1)u_1^2(\zeta,k)dS(\zeta)$$
$$u_2^0(z,k)|_{\partial\Omega} = \frac{e^{-ik\bar{z}}}{-ik}\Big|_{\partial\Omega} - \int_{\partial\Omega} G_0(-\bar{z}+\bar{\zeta})(\Lambda_\gamma - \gamma_1)u_2^0(\zeta,k)dS(\zeta)$$

were computed for $z = z_\ell$, the center of the ℓth electrode, via Simpson's rule, and G_0 was set to 0 when $\zeta = z_\ell$. Note that by the definition of G_0, $G_0(z - \zeta) = G_0(-\bar{z} + \bar{\zeta})$.

3.2.2 Computation of Ψ_{12} and Ψ_{21}—The boundary integral formulas (58) and (59) for Ψ_{12} and Ψ_{21}, respectively, require knowledge of $[\Lambda_\gamma - \Lambda_1]u_j(\zeta,k)$ for $j = 1, 2$, with $\zeta \in \Omega$, and $k \in \mathbb{C}\backslash\{0\}$. These values are already computed during the evaluation of u_1 and u_2 via (45) and (50). Therefore, we merely recall those values and approximate the boundary integral using a finite sum. One should note that $G_0(z - \zeta)$, $\bar{\partial}_z G_k(z - \zeta)$, and $\partial_z G_k(-\bar{z} + \bar{\zeta})$ are all undefined for $z = \zeta$. We removed these points in the computation by setting their values to zero.

3.2.3 Computation of the scattering transform—The off-diagonal entries of the scattering transform matrix, namely $S_{12}(k)$ and $S_{21}(k)$, were computed inside the square $[-K, K]^2$ (with $k = 0$ not included since the formulas for the CGO solutions do not hold for $k = 0$). We compute $S_{12}(k)$ and $S_{21}(k)$ using a finite sum approximation to (56) and (57):

$$S_{12}(k) \approx \frac{i}{L}\sum_{\ell=1}^{L} e^{-i\bar{k}z_\ell}\Psi_{12}(z_\ell,k)z_\ell$$
$$S_{21}(k) \approx -\frac{i}{L}\sum_{\ell=1}^{L} e^{-i\bar{k}\bar{z}_\ell}\Psi_{21}(z_\ell,k)\bar{z}_\ell,$$

where z_l denotes the coordinate of the ℓth equally spaced electrode around Ω (in this case the unit circle).

3.3 Solution of the system of D-bar equations

The two systems of $\bar{\partial}_k$ equations (68) and (69) can be written as the convolutions

$$\begin{cases} 1 = & M_{11}(z,k) - \frac{1}{\pi k} * (M_{12}(z,\bar{k})e(z,-k)S_{21}(k)) \\ 0 = & M_{12}(z,k) - \frac{1}{\pi k} * (M_{11}(z,\bar{k})e(z,\bar{k})S_{12}(k)) \end{cases}, \quad (78)$$

and

$$\begin{cases} 1= & M_{22}(z,k)-\frac{1}{\pi k}*(M_{21}(z,\bar{k})e(z,\bar{k})S_{21}(k)) \\ 0= & M_{12}(z,k)-\frac{1}{\pi k}*(M_{22}(z,\bar{k})e(z,-k)S_{21}(k)) \end{cases}. \quad (79)$$

A numerical solver for equations of the form

$$\bar{\partial}_k v(k)=T(k)\overline{v(k)}.$$

was developed in [36] for the inverse conductivity problem. The solver is based on the fast method by Vainikko [37] that uses FFT's for solving integral equations with weakly singular kernels.

In this work, we must solve the systems of equations (78) and (79) rather than a single equation. Furthermore, the unknowns $M(z, k)$ are not conjugated, but instead the argument k is conjugated. To address this, we interpolated the scattering data S_γ, computed above in Section 3.2.3, to a new k-grid that includes the origin $k = 0$ at the center and has an odd number of grid points in both the horizonal and vertical directions. We solve the systems (78) and (79) on this new k-grid using appropriate flip operations to ensure that we access the correct entries in the matrix corresponding to $M(z, \bar{k})$.

To perform the convolution we used Fourier transforms as follows:

$$\frac{1}{\pi k}*(M_{12}(z,\bar{k})e(z,-k)S_{21}(k))$$
$$=h_\kappa^2\,\mathrm{IFFT}\left(\mathrm{FFT}\left(\frac{1}{\pi k}\right)\cdot\mathrm{FFT}\left(M_{12}(z,\bar{k})e(z,-k)S_{21}(k)\right)\right),$$

and similarly

$$\frac{1}{\pi k}*(M_{11}(z,\bar{k})e(z,\bar{k})S_{12}(k))$$
$$=h_\kappa^2\,\mathrm{IFFT}\left(\mathrm{FFT}\left(\frac{1}{\pi k}\right)\cdot\mathrm{FFT}\left(M_{11}(z,\bar{k})e(z,\bar{k})S_{12}(k)\right)\right),$$

where h_k is the step size of the uniform k-grid of size 129×129, and $\cdot$ denotes componentwise multiplication. We used GMRES to solve the resulting linear systems for each value of z in a grid of 128 equally spaced points between $[-1.1, 1.1]$ in both the x and y directions and computed $M(z, k)$ for all $|z|$ 1.1. The step size in z was $h_z \approx 0.0173$.

3.4 Computation of the admittivity

The admittivity is computed by solving first for Q_{21} from (72) (note that equivalently one could use Q_{12} from (71)), and then solving (77) for $\log(\gamma)$ in the Fourier domain using FFT's. The functions M_+ and M_- in equations (73) and (74) were evaluated using the entries of $M(z, 0)$ recovered when solving the $\bar{}_k$ equation (see Section 3.3 above). We used centered finite differences (with a step size of $h_z \approx 0.0173$) to evaluate the $\bar{}_z$ and $_z$ derivatives of M_+ and M_- respectively. We then performed componentwise division to compute Q_{12} and Q_{21} for $|z|$ 1.1. Finally, the computed $\log(\gamma)$ was exponentiated to recover γ inside the unit disk.

4 Numerical Results

We consider several test problems simulating a simplified cross-section of a human torso. In each example, the admittivity is given by $\gamma = \sigma + i\varepsilon$. That is, the imaginary component includes the temporal angular frequency ω. Since this is a known value, there is no loss of generality in representing γ this way in the simulations. The complete electrode model (CEM), originally described in [14], was implemented in the FEM in order to solve the forward problem. The CEM takes into account both the shunting effect of the electrodes and the contact impedances between the electrodes and tissue. In our computations, Ω was chosen to be a disk of radius $0.15m$, and the FEM computations were performed on a mesh with 4538 triangular elements and 32 equispaced electrodes $0.029m \times 0.024m$ placed on the boundary. The effective contact impedance was chosen to be $z = 0.0057\Omega m^2$ on all electrodes in our simulations. The current amplitude was chosen to be $C = 2mA$, and the applied current patterns are the trigonometric patterns

$$I_\ell^j = \begin{cases} C\cos(j\theta_\ell), & 1 \leq \ell \leq L, \quad 1 \leq j \leq \frac{L}{2} \\ C\sin\left(\left(\frac{L}{2}-j\right)\theta_\ell\right), & 1 \leq \ell \leq L, \quad \frac{L}{2}+1 \leq j \leq L-1, \end{cases} \quad (80)$$

where $\theta_\ell = \frac{2\pi\ell}{L}$, $|e_\ell|$ is the area of the ℓth electrode, I_ℓ is the current on the ℓth electrode, and L denotes the total number of electrodes. As in [28, 18], the currents were normalized to have ℓ-norm of 1, and the voltages were normalized accordingly. Also, the DN map was scaled to represent data collected on the unit disk using the relation $\Lambda_{\gamma,1} = r\Lambda_{\gamma,r}$, where the second subscript represents the radius of the disk.

Where indicated, we added 0.01% Gaussian relative noise to the simulated voltages as follows. Denote the (complex-valued) vector of computed voltage for the j-th current pattern by V^j, let $\eta = 0.0001$ denote the noise level, and N a Gaussian random vector (generated by the randn commmand in MATLAB) that is unique for each use of the notation N. Denoting the noisy data by $\tilde{V}^j$ we then have $\tilde{V}^j = \text{Re}(\tilde{V}^j) + i\,\text{Im}(\tilde{V}^j)$ where

$$\text{Re}(\tilde{V}^j) = \text{Re}(V^j) + \eta \max |\text{Re}(V^j)| N$$
$$\text{Im}(\tilde{V}^j) = \text{Im}(V^j) + \eta \max |\text{Im}(V^j)| N.$$

We solve the boundary integral equations (45) and (50) for the traces of the CGO solutions u_1 and u_2 for $k \in [-K, K]^2$, with K varying for each test problem in this work. The solution $M(z, k)$, to the $\bar{\partial}_k$ equation (66), is computed in parallel by the method described in Section 3.3. The low-pass filtering by taking $k \in [-K, K]^2$ results in smooth functions M_{jp}, $j, p = 1$, 2, which are differentiated by centered finite differences to recover Q_{21}, as described in Section 3.4. The admittivity γ was then computed by (77).

Define the dynamic range of the conductivity, and likewise the permittivity, by

$$\frac{\max \sigma^{(K)} - \min \sigma^{(K)}}{\max \sigma - \min \sigma} \cdot 100\%, \quad (81)$$

where the maximum and minimum values are taken on the computational grid for the reconstruction and $\sigma^{(K)}$ denotes the reconstructed conductivity σ that was computed using a scattering transform computed on the truncated k grid.

4.1 Example 1

The first test problem is an idealized cross-section of a chest with a background admittivity of 1+0i. We do not include units or frequency in these examples, since our purpose is to demonstrate that the equations in this paper lead to a feasible reconstruction algorithm for complex admittivities. Reconstructions from more realistic admittivity distributions or experimental data are the topic of future work. Figure 1 shows the values of the admittivity in the simulated heart and lungs. Noise-free reconstructions with the scattering transform computed on a 128×128 grid for $k \in [−5.5, 5.5]^2$ are found in Figure 2. The reconstruction has a maximum conductivity and permittivity value of $1.1452 + 0.1802i$, occurring in the heart region and a minimum of $0.8286 − 0.0247i$, occurring in the lung region, resulting in a dynamic range of 79% for the conductivity and 60% for the permittivity when the negative permittivity value is set to 0. Although this decreases the dynamic range, we set the permittivity to 0 when it takes on a negative value in any pixel, since physically the permittivity cannot be less than 0. The reconstruction has the attributes of good spatial resolution and good uniformity in the reconstruction of the background and its value.

4.2 Example 2

This second example was chosen with conductivity values the same as in Example 1, but with permittivity values in which the "lungs" match the permittivity of the background. This is motivated by the fact that at some frequencies, physiological features may match that of the surrounding tissue in the conductivity or permittivity component. This example, purely for illustration, mimics that phenomenon. The admittivity values can be found in Figure 3. Noise-free reconstructions with the scattering transform computed on a 128×128 grid for $k \in [−5.5, 5.5]^2$ are found in Figure 4. The maximum value of the conductivity and permittivity occur in the heart region, $1.1429 + 0.1828i$, and the minimum value of the conductivity and permittivity is $0.8271 − 0.0204i$. In this example, the dynamic range is 79% for the conductivity and 61% for the permittivity when the negative permittivity value is set to 0. Again the spatial resolution is quite good, and the background is quite homogeneous, although some small artifacts are present in both the real and imaginary parts.

4.3 Example 3

Example 3 is an admittivity distribution of slightly higher contrast, and a non-unitary background admittivity of $\gamma_0 = 0.8 + 0.3i$. See Figure 5 for a plot of the phantom with admittivity values for the regions. Due to the non-unitary background, the problem was scaled, as was done, for example, in [18, 28], by defining a scaled admittivity $\tilde{\gamma} = \gamma/\gamma_0$ to have a unitary value in the neighborhood of the boundary and scaling the DN map by defining $\Lambda_{\tilde{\gamma}} = \gamma_0 \Lambda_{\gamma}$, solving the scaled problem, and rescaling the reconstructed admittivity. The scattering data for the noise-free reconstruction was computed on a 128×128 grid for $k \in [−5.2, 5.2]$. Noisy data was computed as described above in the beginning of this section, and the scattering data was also computed on a 128×128 grid for $|k|$ 5.5. The reconstructions are found in Figure 6. The maximum and minimum values are given in Table 1. In this example, for the noise-free reconstruction, the dynamic range is 71% for the conductivity and 75% for the permittivity. Again the spatial resolution is quite good. There is some degradation in the image and the reconstructed values in the presence of noise. We chose this noise level to be comparable to that of the 32 electrode ACT3 system at RPI [15]. A thorough study of the effects of noise and stability of the algorithm with respect to perturbations in the data is beyond the scope of this paper. The scattering transform began to blow up for noisy data, requiring a truncation of the admissible scattering data to a circle of radius 5.5, resulting in a dynamic range of 62% for the conductivity and 68% for the permittivity. A thorough study of the effects of the choice of K and its method of selection is not included in this paper.

5 Conclusions

A new direct method is presented for the reconstruction of a complex conductivity. This method has the attributes of being fully nonlinear, parallelizable, and the direct reconstruction does not require a high frequency limit. It was demonstrated on numerically simulated data representing a cross-section of a human chest with discontinuous organ boundaries that the method yields reconstructions with good spatial resolution and dynamic range on noise-free and noisy data. This was the first implementation of such a method, and although efforts were made to realistically simulate experimental data by including discontinuous organ boundaries, data on a finite number of electrodes, and simulated contact impedance, actual experimental data will surely prove more challenging. While this study with simulated data gives very promising results, more advanced studies of stability and robustness may be necessary to deal with the more difficult problem of reconstructions from experimental data.

Acknowledgments

References

1. Astala K, Päivärinta L. Calderón's inverse conductivity problem in the plane. Ann of Math. 2006; 163:265–299.

2. Astala K, Lassas M, Päivärinta L. Calderón's inverse problem for anisotropic conductivity in the plane. Comm Partial Differential Equations. 2005; 30:207–224.

3. Astala K, Mueller JL, Päivärinta L, Siltanen S. Numerical computation of complex geometrical optics solutions to the conductivity equation. Applied and Computational Harmonic Analysis. 2010; 29:2–17.

4. Astala K, Mueller JL, Päivärinta L, Perämäki A, Siltanen S. Direct electrical impedance tomography for nonsmooth conductivities. Inverse Problems and Imaging. 2011; 5:531–550.

5. Barceló JA, Barceló T, Ruiz A. Stability of the Inverse Conductivity Problem in the Plane for Less Regular Conductivities. J Differential Equations. 2001; 173:231–270.

6. Bikowski J, Mueller JL. 2D EIT reconstructions using Calderón's method. Inverse Problems and Imaging. 2008; 2:43–61.

7. Borcea L. Electrical impedance tomography. Inverse Problems. 2002; 18:99–136.

8. Boverman G, Kao T-J, Kulkarni R, Kim BS, Isaacson D, Saulnier GJ, Newell JC. Robust linearized image reconstruction for multifrequency EIT of the breast. IEEE Trans Biomed Eng. 2008; 27:1439–1448.

9. Brown BH, Barber DC, Morice AH, Leathard A, Sinton A. Cardiac and respiratory related electrical impedance changes in the human thorax. IEEE Trans Biomed Eng. 1994; 41:729–734. [PubMed: 7927395]

10. Brown RM, Uhlmann G. Uniqueness in the inverse conductivity problem for nonsmooth conductivities in two dimensions. Comm Partial Differential Equations. 1997; 22:1009–1027.

11. Bukhgeim AL. Recovering a potential from cauchy data in the two-dimensional case. Inverse Problems. 2007; 15:1–15.

12. Calderón AP. On an inverse boundary value problem. In Seminar on Numerical Analysis and its Applications to Continuum Physics. Soc Brasileira de Matemàtica. 1980:65–73.

13. Cheney M, Isaacson D, Newell JC. Electrical Impedance Tomography. SIAM Review. 1999; 41:85–101.

14. Cheng K-S, Isaacson D, Newell JC, Gisser DG. Electrode models for electric current computed tomography. IEEE Trans on Bio Eng. 1989; 36(9):918–924.

15. Cook RD, Saulnier GJ, Goble JC. A phase sensitive voltmeter for a high-speed, high precision electrical impedance tomograph. Proc Ann Int Conf IEEE Eng in Medicine and Biology Soc. 1991:22–23.

16. Costa ELV, Chaves CN, Gomes S, Gonzalez Lima R, Amato MBP. Real-time detection of pneumothorax using electrical impedance tomography. Crit Care Med. 2008; 36:1230–1238. [PubMed: 18379250]

17. Costa ELV, Gonzalez Lima R, Amato MBP. Electrical impedance tomography. Current Opinion in Crit Care. 2009; 15:18–24.

18. DeAngelo M, Mueller JL. D-bar reconstructions of human chest and tank data using an improved approximation to the scattering transform. Physiological Measurement. 2010; 31:221–232. [PubMed: 20057005]

19. Edic PM, Isaacson D, Saulnier GJ, Jain H, Newell JC. An iterative Newton-Raphson method to solve the inverse admittivity problem. IEEE Trans Biomed Engr. 1998; 45:899–908.

20. Faddeev LD. Increasing solutions of the Schrödinger equation. Sov Phys Dokl. 1966; 10:1033–1035.

21. Francini E. Recovering a complex coefficient in a planar domain from the Dirichlet-to-Neumann map. Inverse Problems. 2000; 6:107–119.

22. Frerichs I, Hinz J, Herrmann P, Weisser G, Hahn G, Dudykevych T, Quintel M, Hellige G. Detection of local lung air content by electrical impedance tomography compared with electron beam CT. J Appl Physiol. 2002; 93(2):660–6. [PubMed: 12133877]

23. Frerichs I, Hinz J, Herrmann P, Weisser G, Hahn G, Quintel M, Hellige G. Regional lung perfusion as determined by electrical impedance tomography in comparison with electron beam CT imaging. IEEE Trans Med Imaging. 2002; 21:646–652. [PubMed: 12166861]

24. Frerichs I, Schmitz G, Pulletz S, Schädler D, Zick G, Scholz J, Weiler N. Reproducibility of regional lung ventilation distribution determined by electrical impedance tomography during mechanical ventilation. Physiol Meas. 2007; 28:261–267.

25. Fuks LF, Cheney M, Isaacson D, Gisser DG, Newell JC. Detection and Imaging of Electric conductivity and permittivity at low frequency. IEEE Trans Biomed Engr. 1991; 38:1106–1110.

26. Hamilton, SJ. PhD thesis. Colorado State University; 2012. A Direct D-bar Reconstruction Algorithm for Complex Admittivities in $W^{2,\infty}(\Omega)$ for the 2-D EIT Problem.

27. Mueller JL, Siltanen S, Isaacson D. A Direct Reconstruction Algorithm for Electrical Impedance Tomography. IEEE Trans Med Im. 2003; 21:555–559.

28. Isaacson D, Mueller JL, Newell JC, Siltanen S. Reconstructions of chest phantoms by the D-bar method for electrical impedance tomography. IEEE Trans Med Im. 2004; 23:821–828.

29. Isaacson D, Mueller JL, Newell JC, Siltanen S. Imaging cardiac activity by the D-bar method for electrical impedance tomography. Physiol Meas. 2006; 27:S43–S50. [PubMed: 16636419]

30. Jain H, Isaacson D, Edic PM, Newell JC. Electrical impedance tomography of complex conductivity distributions with noncircular boundary. IEEE Trans Biomed Engr. 1997; 44:1051–1060.

31. Kao T-J, Boverman G, Kim BS, Isaacson D, Saulnier GJ, Newell JC, Choi MH, Moore RH, Kopans DB. Regional admittivity spectra with tomosynthesis images for breast cancer detection: preliminary patient study. IEEE Trans Med Im. 2008; 27:1762–1768.

32. Kerner TE, Paulsen KD, Hartov A, Soho SK, Poplack SP. Electrical Impedance Spectroscopy of the Breast: Clinical Imaging Results in 26 Subjects. IEEE Trans Med Im. 2002; 21:638–645.

33. Knudsen, K. PhD thesis. Department of Mathematical Sciences, Aalborg University; Denmark: 2002. On the Inverse Conductivity Problem.

34. Knudsen K. A new direct method for reconstructing isotropic conductivities in the plane. Physiol Meas. 2003; 24:391–401. [PubMed: 12812424]

35. Knudsen K, Tamasan A. Reconstruction of less regular conductivities in the plane. Comm Partial Differential Equations. 2004; 29:361–381.

36. Knudsen K, Mueller JL, Siltanen S. Numerical solution method for the dbar-equation in the plane. J Comp Phys. 2004; 198:500–517.

37. Vainikko, G. In Direct and inverse problems of mathematical physics (Newark, DE, 1997), volume 5 of Int Soc Anal Appl Comput. Kluwer Acad. Publ; Dordrecht: 2000. Fast solvers of the Lippmann-Schwinger equation; p. 423-440.

38. Knudsen K, Lassas M, Mueller JL, Siltanen S. Reconstructions of piecewise constant conductivities by the D-bar method for electrical impedance tomography, Proceedings of the 4th AIP International Conference and the 1st Congress of the IPIA, Vancouver. Journal of Physics: Conference Series. 2008; 124

39. Knudsen K, Lassas M, Mueller JL, Siltanen S. D-bar method for electrical impedance tomography with discontinuous conductivities. SIAM J Appl Math. 2007; 67:893–913.

40. Knudsen K, Lassas M, Mueller JL, Siltanen S. Regularized D-bar method for the inverse conductivity problem. Inverse Problems and Imaging. 2009; 3:599–624.

41. Mueller JL, Siltanen S. Direct reconstructions of conductivities from boundary measurements. SIAM J Sci Comp. 2003; 24:1232–1266.

42. Murphy E, Mueller JL, Newell JC. Reconstruction of conductive and insulating targets using the D-bar method on an elliptical domain. Physiol Meas. 2007; 28:S101–S114. [PubMed: 17664628]

43. Nachman AI. Reconstructions from boundary measurements. Annals of Mathematics. 1988; 128:531–576.

44. Nachman AI. Global uniqueness for a two-dimensional inverse boundary value problem. Ann of Math. 1996; 143:71–96.

45. Nachman, AI. University of Rochester, Dept of Mathematics Preprint Series, No. 19. 1993. Global uniqueness for a two-dimensional inverse boundary value problem.

46. Siltanen S, Mueller J, Isaacson D. An implementation of the reconstruction algorithm of A. Nachman for the 2-D inverse conductivity problem. Inverse Problems. 2000; 16:681–699.

47. Siltanen, S. PhD Thesis. Helsinki University of Technology; Espoo, Finland: 1999. Electrical Impedance Tomography and Faddeev Green's Functions.

48. Smit H, Vonk Noordegraaf A, Marcus JT, Boonstra A, de Vries PM, Postmus PE. Determinants of pulmonary perfusion measured by electrical impedance tomography. Eur J Appl Physiol. 2004; 92:45–49. [PubMed: 14985995]

49. Sylvester J, Uhlmann G. A global uniqueness theorem for an inverse boundary value problem. Annals of Mathematics. 1987; 125:153–169.

50. Tidswell AT, Gibson A, Bayford RH, Holder DS. Three-dimensional electrical impedance tomography of human brain activity. NeuroImage. 2001; 13:283–294. [PubMed: 11162269]

51. Tidswell AT, Gibson A, Bayford RH, Holder DS. Validation of a 3D reconstruction algorithm for EIT of human brain function in a realistic head-shaped tank. Physiological Meas. 2001; 22:177–185.

52. Victorino JA, Borges JB, Okamoto VN, Matos GFJ, Tucci MR, Caramez MPR, Tanaka H, Santos DCB, Barbas CSV, Carvalho CRR, Amato MBP. Imbalances in Regional Lung ventilation: a validation study on electrical impedance tomography. Am J Respir Crit Care Med. 2004; 169:791–800. [PubMed: 14693669]

53. Von Herrmann, A. PhD thesis. Colorado State University; 2009. Properties of the reconstruction algorithm and associated scattering transform for admittivity $\gamma \in W^{1,p}(\Omega)$ in the plane.
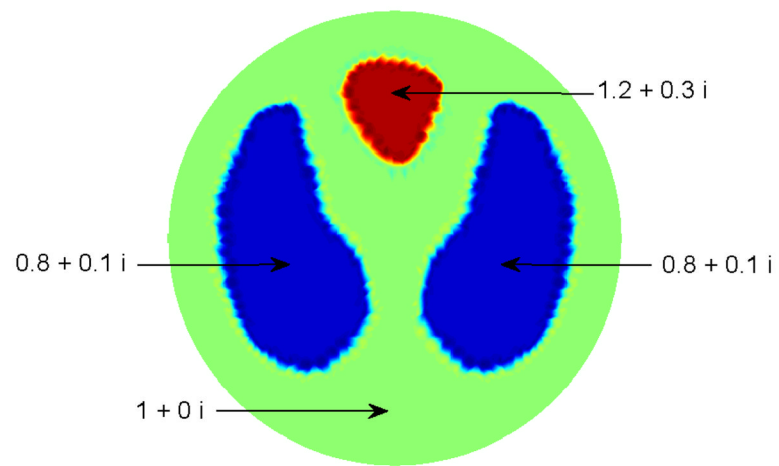
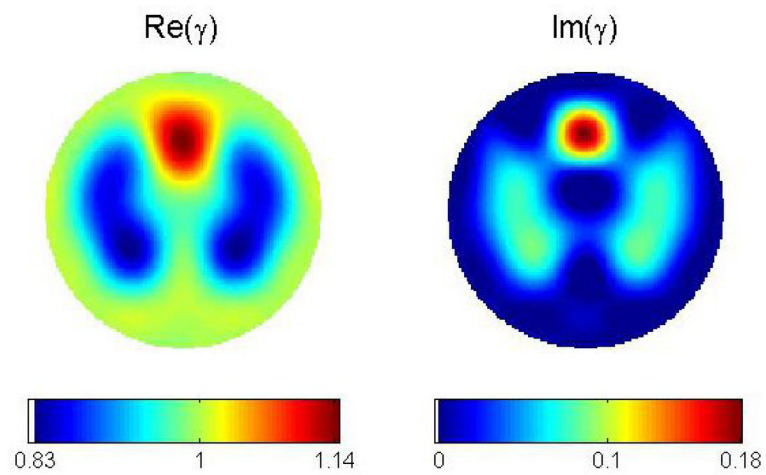**Figure 1.**
The test problem in Example 1.

Figure 2.
Reconstruction from noise-free data for Example 1 with the real part of γ (conductivity) on the left, and the imaginary part (permittivity) on the right. The cut-off frequency was $K = 5.5$. The dynamic range is 79% for the conductivity, and 60% for the permittivity.
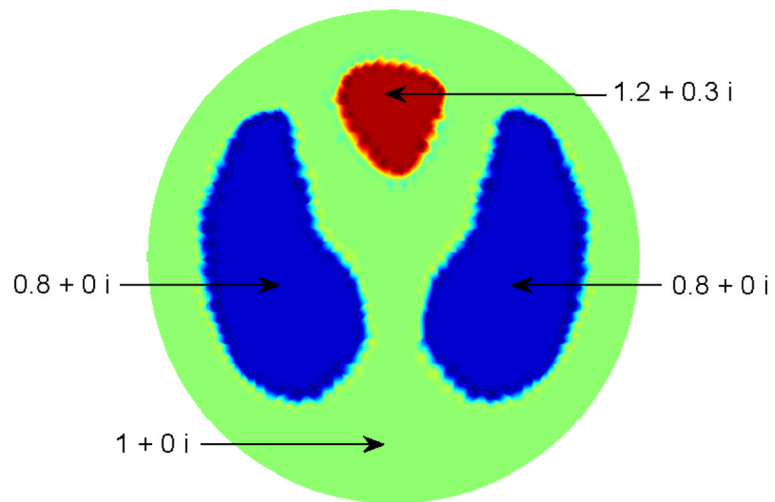
Figure 3.
The test problem in Example 2. Notice that in this case, the permittivity of the lungs matches the permittivity of the background, and so only the heart should be visible in the imaginary component of the reconstruction.
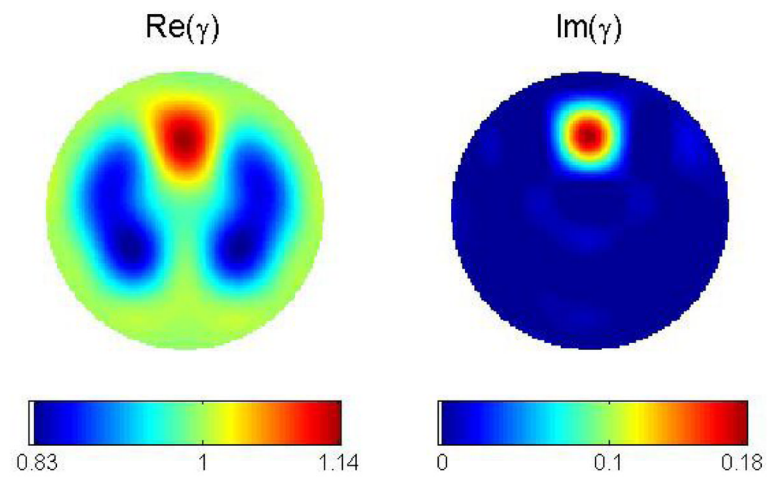
Figure 4.
Reconstruction from noise-free data for Example 2 with the real part of γ (conductivity) on the left, and the imaginary part (permittivity) on the right. The cut-off frequency was $K = 5.5$. The dynamic range is 79% for the conductivity, and 61% for the permittivity.
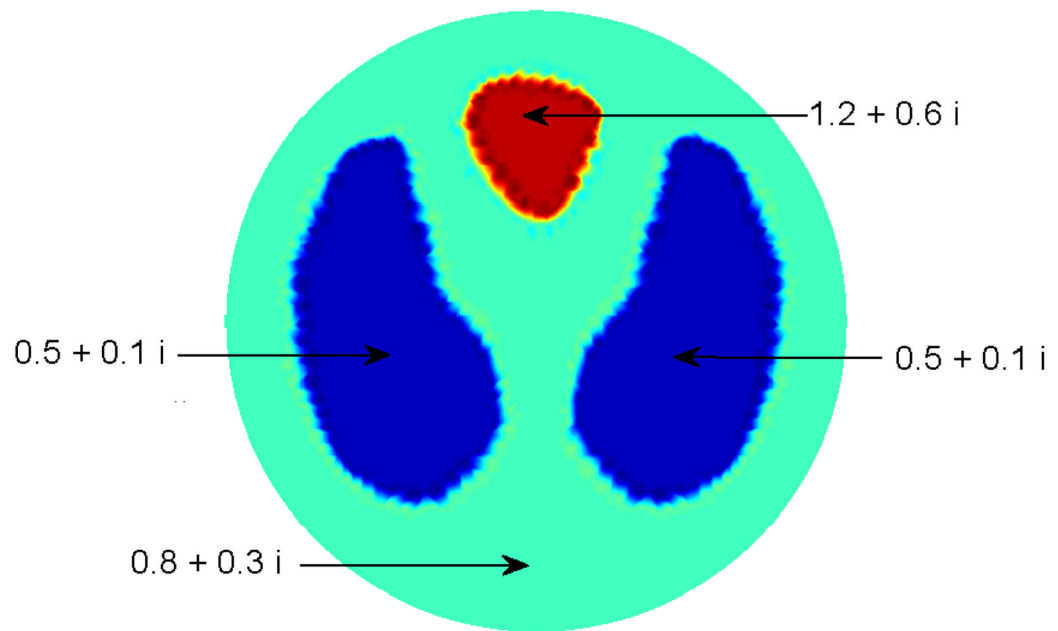
Figure 5.
The test problem in Example 3. In this case, the background admittivity is $0.8 + 0.3i$, rather than $1 + 0i$ as in Examples 1 and 2.
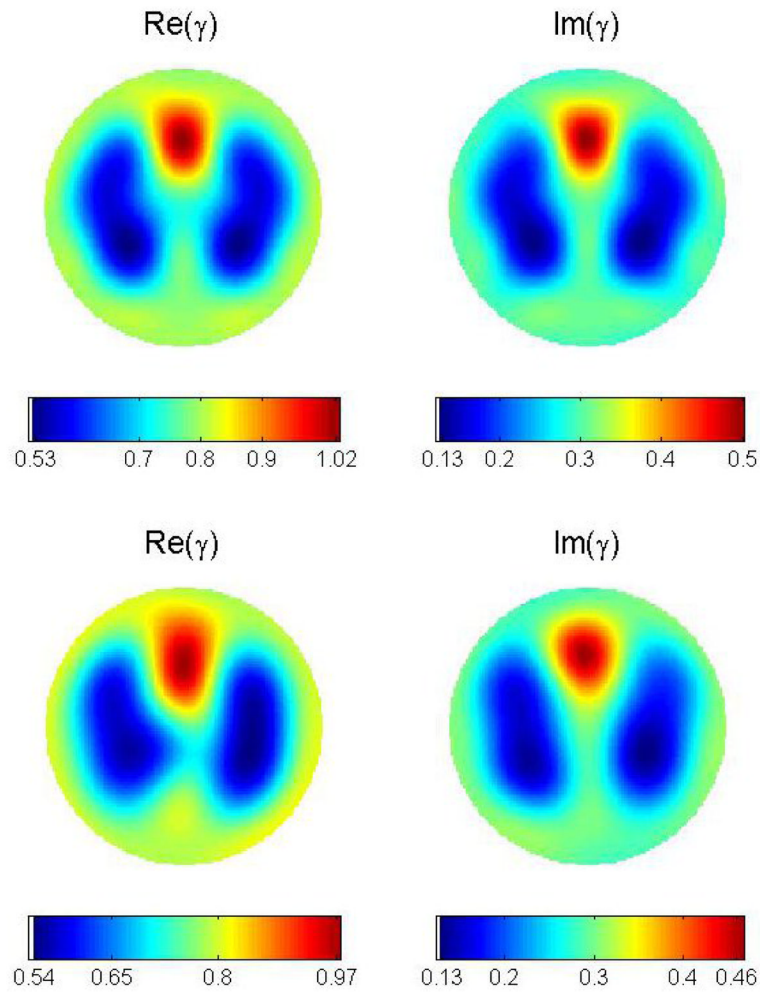
Figure 6.
Top row: Reconstruction from noise-free data for Example 3. The cut-off frequency was $K =$ 5.2. The dynamic range is 71% for the conductivity, and 75% for the permittivity. Bottom row: Reconstruction from data with 0.01% added noise. The cut-off frequency was $|k|$ 5.5. The dynamic range is 62% for the conductivity, and 68% for the permittivity.

Table 1

Maximum and minimum values in Example 3 with the non-unitary background were found in the appropriate organ region. The table indicates these values of the admittivity in the appropriate region.

	Admitivity of test problem	Reconstruction from noise-free data	Reconstruction from noisy data
heart	1.2 + 0.6 i	1.0246 + 0.5014 i (max)	0.9740 + 0.4679 i (max)
lungs	0.5 + 0.1i	0.5262 + 0.1258 i (min)	0.5390 + 0.1281 i (min)